RSC Advances

PAPER

View Article Online
View Journal | View Issue

Cite this: *RSC Adv.*, 2017, **7**, 9628

N_2O-emission-free exhaust remediation by Rh-NbO_x nanocomposites developed from Rh_3Nb alloy precursor†

Tsubasa Imai,[ab] Shigenori Ueda,[c] Satoshi Nagao,[d] Hirohito Hirata,[d] Koolath Ramakrishnan Deepthi[e] and Hideki Abe*[a]

Received 22nd November 2016
Accepted 13th January 2017

DOI: 10.1039/c6ra27168e

rsc.li/rsc-advances

Metal-oxide nanocomposites comprising rhodium (Rh) nanoparticles (<50 nm) and oxygen-deficient niobium oxides (NbO_x: x < 5/2) were developed from Rh_3Nb alloy precursors. The Rh-NbO_x nanocomposite exhibited enhanced activity toward the catalytic remediation of nitrogen oxide (NO) in the presence of carbon monoxide (CO) without emissions of nitrous oxide (N_2O) due to the promoted dissociation of NO admolecules at the Rh/NbO_x interface.

Green-house gases, such as carbon dioxide (CO_2), are becoming a serious hazard for the world's environment.[1] In particular, nitrous oxide (N_2O) is a universal issue because of its ability to absorb infrared light and is contributes 200 fold more than CO_2 to global warming.[2] Currently, 1.5% of atmospheric N_2O is released as part of nitrogen oxides (NO_x: N_2O, NO, N_2O_5 and NO_2) contained in automobile exhaust.[3] The NO_x are remediated to environmentally benign nitrogen (N_2) through redox reactions with carbon monoxide (CO) that is produced by the incomplete combustion of fuels (NO_x remediation).[4] Nanoparticles of precious-group metals (PGM), particularly rhodium (Rh), are widely used as the catalyst for the NO_x remediation.[5] However, the current Rh catalysts preferentially promote the partial reduction of NO to N_2O (*i.e.*, $NO + 1/2CO = 1/2N_2O + 1/2CO_2$) instead of the desired NO_x remediation, when applied to the low-temperature exhaust (<350 °C) from hybrid engines or two-stroke engines of motorcycles.[6] In order to meet the demands for hybrid cars and motorcycles in the advanced and emerging countries, respectively, it is of growing importance to develop high-performance NO_x remediation catalysts for the low-temperature exhaust without N_2O emissions.[7]

It is acknowledged that Rh nanoparticles exhibit enhanced performance for either the catalytic decomposition of N_2O (*i.e.*, $N_2O = N_2 + 1/2O_2$) or the low-temperature NO_x remediation, when finely dispersed and immobilized on oxide-based supporting materials (supported Rh catalysts).[8] $Al_6Si_2O_{13}$ (Mullite)-supported Rh nanoparticles efficiently decomposed N_2O at 350 °C or higher temperatures.[9] Supporting materials comprising cerium-doped Al_2O_3 realized the N_2O decomposition even at 250 °C.[10] It was also demonstrated that the Rh nanoparticles supported on cerium-zirconium oxides ($(Ce_{1-x}Zr_x)O_y$; $y < 2$) remediated the NO_x at 250 °C or higher temperatures. Rh nanoparticles supported on aluminium phosphate ($AlPO_4$) showed an improved low-temperature activity toward the NO_x remediation.[10] However, none of these Rh catalysts has achieved the desired low-temperature NO_x remediation without N_2O emission.

Herein, we report that the N_2O emission-free, low-temperature NO_x remediation can be realized by a nanocomposite of Rh metal and niobium oxide (*i.e.* Rh@NbO_x) that was developed from a Rh–Nb alloy precursor (*i.e.* Rh_3Nb) through controlled annealing in a gas mixture comprising NO and CO. Powder X-ray diffraction (pXRD), hard X-ray photoemission spectroscopy (HAXPES) and transmission-electron microscopy (TEM) have demonstrated that Rh@NbO_x consisted of interconnected Rh nanoparticles (particle size < 50 nm) that were further incorporated in a matrix of oxygen-deficient niobium oxide (NbO_x; x < 2.5). *In situ* X-ray photoemission spectroscopy (*in situ* XPS) has shown that the NbO_x matrix can dissociate NO_{ad} at room temperature through the formation of N–Nb bonds at the Rh/NbO_x interface. As a result of the promoted NO_{ad} dissociation, the Rh@NbO_x efficiently catalysed the remediation of NO to N_2 ($NO + CO = 1/2\ N_2 + CO_2$) without N_2O emission at low temperatures.

Pure-phased Rh_3Nb ingots were first synthesized using arc-melting elemental metals in pure Ar atmosphere. The Rh_3Nb ingot was then powdered to an average particle size of 50 μm. The obtained Rh_3Nb powder was exposed to a He-balanced stream of NO/CO gas mixture at elevated temperatures up to

[a]*National Institute for Materials Science, 1-1 Namiki, Tsukuba, Ibaraki 305-0044, Japan*

[b]*Graduate School of Science and Technology, Saitama University, 255 Shimo-Okubo, Saitama 338-8570, Japan*

[c]*Synchrotron X-ray Station at SPring-8, National Institute for Materials Science, 1-1-1 Kouto, Sayo, Hyogo, 679-5148, Japan*

[d]*Toyota Motor Corporation, Mishuku 1200, Susono, Shizuoka 410-1107, Japan*

[e]*Crystal Growth Centre, Anna University, Chennai, Tamil Nadu 600-025, India*

† Electronic supplementary information (ESI) available. See DOI: 10.1039/c6ra27168e

600 °C (NO : CO : He = 1 : 1 : 98 in volume) to convert the Rh_3Nb precursor to the desired Rh@NbO_x nanocomposite (see ESI for details†).

Fig. 1 shows the powder X-ray diffraction (pXRD) profiles for the Rh_3Nb precursor and the Rh@NbO_x nanocomposite. The pXRD peaks for the Rh_3Nb precursor were located at 40.43, 47.02, 68.74, 82.86 and 87.44 degrees, which corresponded to the 111-, 200-, 220-, 311- and 322 reflections of the cubic Au_3Cu structure ($Pm\bar{3}m$, a = 0.3865 nm), respectively.[11] After the exposure to the NO/CO gas mixture, the pXRD peaks shifted toward higher diffraction angles as a result of phase separation of the uniform alloy into the nanocomposite consisting of Rh and NbO_x. The major reflections from the Rh@NbO_x were observed at 40.92, 47.62, 69.98, 84.19 and 88.93 degrees, corresponding to the 111-, 200-, 220-, 311- and 322 reflections of the face-center cubic (FCC) structure of Rh metal ($Fm\bar{3}m$, a = 0.3804 nm).[12] In addition to the intense reflections from the Rh phase, there were recognized weak and broad reflections from a NbO_x phase with the crystal structure identical to that of niobium pentoxide, Nb_2O_5.[13]

To investigate the chemical state of the Rh@NbO_x nanocomposite, we conducted hard X-ray photoemission spectroscopy (HAXPES; photon energy = 5.9534 keV). Fig. 2a shows the HAXPES spectra for the Rh_3Nb precursor and the Rh@NbO_x in the Nb 3d region. The Nb $3d_{5/2}$- and $3d_{3/2}$ photoemission peaks for the Rh_3Nb were located at the binding energy of 203.0 and 205.9 eV, respectively.[14] The corresponding peaks for the Rh@NbO_x were located at the peak positions of 206.9 and 209.7 eV, showing that the Nb cations had a valence close to +5.[15]

The HAXPES spectra in the Rh 3d region are presented in Fig. 2b. The Rh $3d_{5/2}$ peaks for the Rh_3Nb precursor and pure Rh metal were observed at different binding energies, 306.5 and 307.0 eV, respectively. The Rh@NbO_x showed a Rh $3d_{5/2}$ peak at 306.7 eV, in between those for the Rh_3Nb alloy precursor and pristine Rh, indicating the metallic nature of the Rh phase included in the Rh@NbO_x. The intense photoemission at 307.9 eV was assigned to a thin oxide layer ($Rh^{3+}O_y$) over the Rh surface because the emission was prominent when probed with surface-sensitive XPS (photon energy = 1.4866 keV; see Fig. S1†).

The nanostructure of the Rh@NbO_x was investigated with a scanning transmission electron microscope (STEM) equipped with an energy-dispersion spectrometer (EDS) (Fig. 3, see also Fig. S2–S4† for STEM/TEM images). It was demonstrated that Rh was distributed in the bulk and/or over the surface of the Rh@NbO_x as nanoparticles with an average size of 50 nm. Importantly, the Rh nanoparticles were connected to each other to form a network structure. The distributions of Nb and O were exclusive to that of Rh, showing that Nb and O formed a NbO_x phase. Most of the Rh network was incorporated in the NbO_x matrix and partly exposed to the atmosphere (see Fig. S5† for the scanning-electron microscope (SEM) images of the Rh@NbO_x). The Rh exposure was surrounded by the NbO_x matrix over the catalyst surface, forming a metal/oxide interface around its perimeter.

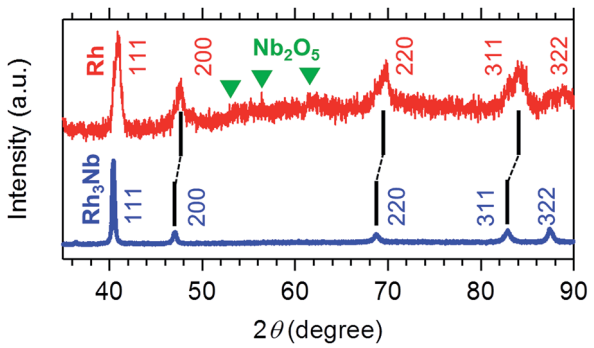

Fig. 1 Powder X-ray diffraction (pXRD) profiles for the Rh_3Nb precursor (blue) and the developed Rh@NbO_x nanocomposite (red). The green triangles correspond to the reflections from Nb_2O_5.

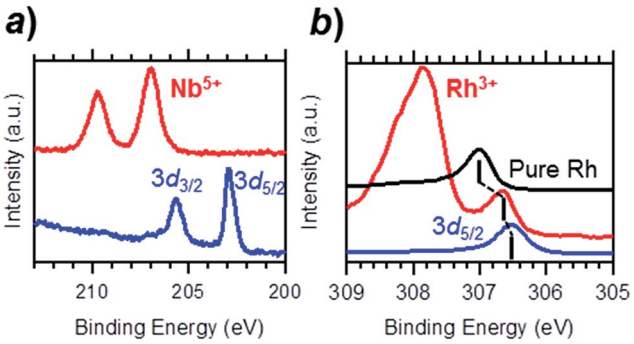

Fig. 2 Hard X-ray photoemission spectroscopy (HAXPES) profiles for the Rh_3Nb precursor (blue) and the Rh@NbO_x (red) in the (a) Nb 3d- and (b) Rh 3d regions.

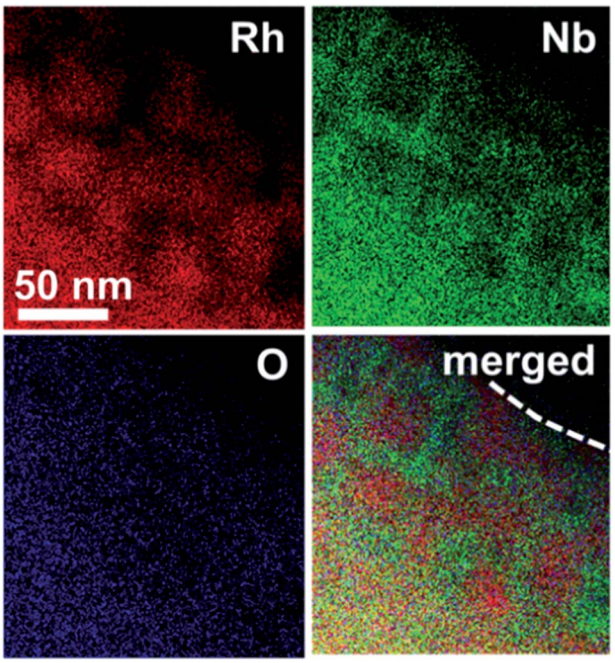

Fig. 3 Compositional mapping images of the Rh@NbO_x acquired with a scanning transmission microscope (STEM) equipped with an energy-dispersive spectrometer (EDS). The broken curve in the merged image corresponds to the interface between the materials surface and the atmosphere.

Fig. 4 shows the exhaust-remediation performance of the Rh@NbO_x and the control Rh catalyst (see ESI for the experimental details†). The Rh- and Rh@NbO_x catalysts were subjected to a steady stream of simulated exhaust (NO : CO : He = 1 : 1 : 98 in volume%; space velocity = 30 000 h^{-1}; flow rates of NO and CO = 5 μmol min^{-1}) at different temperatures from 200 to 400 °C (see Fig. S6† for the FTIR spectra for the effluent gas).

The Rh catalyst converted NO to N_2 and/or N_2O at 250 °C and higher temperatures (Fig. 4a). The flow rate of N_2O in the effluent gas was 1.1 μmol min^{-1} at 250 °C, showing that 44% of the incoming NO was converted to N_2O (see bar charts in the inset). The conversion rate from NO to N_2O still remained 13% at 300 °C (inset). The residual N_2O disappeared from the effluent gas when the temperature exceeded 350 °C. By clear contrast to the trend observed for the Rh catalyst, the Rh@NbO_x remediated NO with much lowered N_2O emission (Fig. 4b). The N_2O concentration in the effluent gas was less than 2% at 250 °C or higher temperatures (see insets). Moreover, the Rh@NbO_x fully converted NO to N_2 at 300 °C or higher temperatures. Considering the experimental data and the reported lower performance of the palladium-based catalysts than that of Rh-based catalysts, we concluded that the Rh@NbO_x was superior to the state-of-the-art PGM catalysts for the N_2O emission-free NO remediation at low temperatures.[16]

Finally, *in situ* X-ray photoemission spectroscopy (*in situ* XPS) was conducted to reveal the mechanism behind the N_2O emission-free NO remediation over the Rh@NbO_x catalyst. A polycrystalline Rh_3Nb sample was polished to a mirror finish prior to use in the experiments. Single-crystalline Rh was sliced and mirror-polished to develop the (111) surface (see ESI for details†). The samples were introduced into an ultra-high vacuum (UHV) chamber, cleaned by Ar^+ bombardment and exposed to NO gas up to one-monolayer adsorption (1.0 L) at room temperature. The NO-adsorbed sample surfaces were then observed using an XPS spectrometer (monochromatized AlKα; photon energy = 1.4866 keV) in the N 1s- and O 1s regions at elevated temperatures from room temperature to 800 °C.

Fig. 5a shows a contour plot of the N 1s photoemission intensity for the Rh(111) surface as a function of temperature

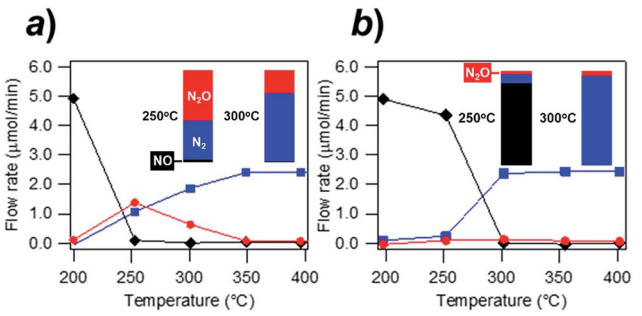

Fig. 4 Remediation of simulated exhaust (NO : CO : He = 1 : 1 : 98 vol%) at different temperatures using the (a) Rh catalyst and (b) Rh@NbO_x catalyst. The black, blue and red curves respectively correspond to the flow rates of NO, N_2 and N_2O in the effluent gas. Bar charts in the insets show the nitrogen concentration (%) in the flows of NO, N_2 or N_2O at 250 and 300 °C.

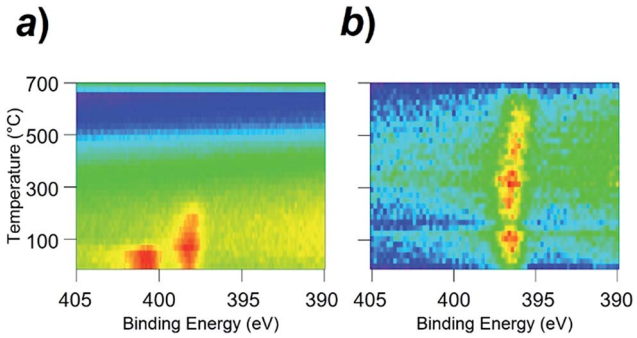

Fig. 5 *In situ* X-ray photoemission spectra (*in situ* XPS) for (a) the clean Rh surface and (b) Rh_3Nb surface. In terms of colour, red indicates high intensity, blue indicates low intensity.

and binding energy. At room temperature, the N 1s emission peak was located at the binding energy of 400.6 eV. This value is assigned to the NO molecules adsorbed onto the Rh surface (NO_{ad}).[11] With an increase in the surface temperature, the N 1s peak was 2.5 eV shifted at 100 °C toward the lower binding energy, as the result of the dissociation of NO_{ad} into N_{ad} and O_{ad} (see Fig. S7†for the *in situ* XPS spectra in the O 1s region).[11] The N_{ad} was thermally desorbed from the surface when the temperature reached 250 °C, diminishing the N 1s emission.

Unlike the Rh surface, as seen in Fig. 5b, the N 1s-emission peak from the NO-adsorbed Rh_3Nb surface was located at 396.8 eV at room temperature, which corresponds to the atomic N_{ad} instead of the molecular NO_{ad}. This binding energy (396.8 eV) is close to the value for the N 1s emissions from niobium nitride (NbN) and/or niobium oxynitride (NbON), 396.2 eV.[15] The Rh_3Nb precursor adopted dissociative adsorption of NO to develop the Rh@NbO_x phase on the surface, and the nitrogen adatoms were adsorbed not on the Rh site but on the Nb site to form N–Nb bonds.

One of the major paths for the catalytic N_2O generation is the combination of NO_{ad} and N_{ad} over the catalyst surface (NO_{ad}–N_{ad} reaction: $NO_{ad} + N_{ad} = N_2O$).[17] The low performance of the traditional Rh catalysts for the N_2O emission-free NO_x remediation is ultimately due to the limited ability of the Rh surface dissociating the NO_{ad} only at temperatures higher than 100 °C.[18] The Rh@NbO_x catalyst can efficiently promote the NO_{ad} dissociation because the NbO_x matrix adopts the N_{ad} from the Rh surface to form thermodynamically stable NbON at the Rh/NbO_x interface.[19] Indeed, the Rh@NbO_x catalyst containing larger Rh grains and fewer Rh/NbO_x interfaces on the surface (Fig. S8†) did not realize the desired N_2O-free NO remediation.

Conclusion

In conclusion, we successfully materialized a catalytic nanocomposite comprising nanometer-thick Rh networks and oxygen-deficient NbO_x matrices, namely Rh@NbO_x, by annealing an Rh_3Nb alloy precursor in the NO/CO atmosphere. The synthesized Rh@NbO_x nanocomposite exhibited higher catalytic performance than that of pristine Rh catalysts toward the N_2O emission-free NO remediation. The enhanced performance of the Rh@NbO_x catalyst was attributed to the promoted NO

dissociation due to the formation of N–Nb bonds at the metal/oxide interface. The N_2O emission-free NO remediation using the Rh@NbO_x catalyst will prompt further research and development for high-performance nanocomposite catalysts, realizing reduced impacts to the global atmosphere.

Acknowledgements

This study was preliminarily supported by Toyota Motor Corporation and the JST PRESTO program "New Materials Science and Element Strategy". The HAXPES measurements were performed under the approval of the NIMS Synchrotron X-ray Station (Proposal No. 2015B4605). This study was also supported by NIMS microstructural characterization platform as a program of "Nanotechnology Platform" of the Ministry of Education, Culture, Sports, Science and Technology (MEXT), Japan.

References

1 A. M. Appel, J. E. Bercaw, A. B. Bocarsly, H. Dobbek, D. L. Dubois, M. Dupuis, J. G. Ferry, E. Fujita, R. Hille, P. J. A. Kenis, C. A. Kerfeld, R. H. Morris, C. H. F. Peden, A. R. Portis, S. W. Ragsdale, T. B. Rauchfuss, J. N. H. Reek, L. C. Seefeldt, R. K. Thauer and G. L. Waldrop, *Chem. Rev.*, 2013, **113**, 6621–6658.

2 (*a*) D. A. Lashof and D. R. Ahuja, *Nature*, 1990, **344**, 529–531; (*b*) J. T. Houghton, Y. Ding, D. J. Griggs, M. Noguer, P. J. van der Linden, X. Dai, K. Maskel and C. A. Johnson, *Climate change 2001: the scientific basis*. Cambridge University Press, New York, 2001; (*c*) *IPCC Fourth Assessment Report, Table 2.14*, ch. 2, p. 212; (*d*) M. Li, X. Wu, Y. Cao, S. Liu, D. Weng and R. Ran, *J. Colloid Interface Sci.*, 2013, **408**, 157–163; (*e*) R. G Tonkyn, S. E. Barlow and J. W. Hoard, *Appl. Catal., B*, 2003, **40**, 207–217.

3 IPCC AR4 SYR Appendix Glossary, Retrieved 14 December 2008.

4 M. Shelef and R. W. McCabe, *Catal. Today*, 2000, **62**, 35–50.

5 (*a*) V. I. Parvulescu, P. Grange and B. Delmon, *Catal. Today*, 1998, **46**, 233–316; (*b*) M. Shelef and G. W. Graham, *Catal. Rev.: Sci. Eng.*, 1994, **36**, 433–457.

6 (*a*) P. Z. Zhdanov, *Surf. Sci. Rep.*, 1997, **29**, 31–90; (*b*) Q. Su, Y. Li, S. Wang and C. Gao, *Top. Catal.*, 2013, **56**, 345–351.

7 (*a*) http://www.theicct.org/real-world-exhaust-emissions-modern-diesel-cars, 2014; (*b*) J. Lelieveld, J. S. Evans, M. Fnais, D. Giannadaki and A. Pozzer, *Nature*, 2015, **525**, 367–371.

8 P. Fornasiero, G. Ranga Rao, J. Kaspar, F. L'Erario and M. Graziani, *J. Catal.*, 1998, **175**, 269–279.

9 X. Zhao, Y. Cong, F. Lv, L. Li, X. Wang and T. Zhang, *Chem. Commun.*, 2010, **46**, 3028–3030.

10 (*a*) S. S. Kim, S. J. Lee and S. C. Hong, *Chem. Eng. J.*, 2011, **169**, 173–179; (*b*) M. Li, W. X. Wu, Y. Cao, S. Liu, D. Weng and R. Ran, *J. Colloid Interface Sci.*, 2013, **408**, 157–163.

11 A. E. Dwight and P. A. Beck, *Trans. Metall. Soc. AIME*, 1959, **215**, 976–979.

12 B. C. Giessen, H. Ibach and N. J. Grant, *Trans. Metall. Soc. AIME*, 1964, **230**, 113–122.

13 B. M. Gatehouse and A. D. Wadsley, *Acta Crystallogr.*, 1964, **17**, 1545–1554.

14 (*a*) V. I. Nefedov, M. N. Firsov and I. S. Shaplygin, *J. Electron Spectrosc. Relat. Phenom.*, 1982, **26**, 65–78; (*b*) R. Fontaine, R. Caillat, L. Feve and M. J. Guittet, *J. Electron Spectrosc. Relat. Phenom.*, 1977, **10**, 349–357.

15 A. Darlinski and J. Halbritter, *Surf. Interface Anal.*, 1987, **10**, 223–237.

16 (*a*) S. Salasc, M. Skoglundh and E. Fridell, *Appl. Catal., B*, 2002, **36**, 145–160; (*b*) Y. Su, K. S. Kabin, M. P. Harold and M. D. Amiridis, *Appl. Catal., B*, 2007, **71**, 207–215; (*c*) H. Abdulhamid, J. Dawody, E. Fridell and M. Skoglundh, *J. Catal.*, 2006, **244**, 169–182.

17 L. Kubiak, R. Matarrese, L. Castoldi, L. Lietti, M. Daturi and P. Forzatti, *Study of N_2O formation over Rh- and Pt-based LNT catalysts*, MDPI, 2016.

18 R. J. Baird, R. C. Ku and P. Wynblatt, *Surf. Sci.*, 1980, **97**, 346–362.

19 V. Schwartz and S. T. Oyama, *Chem. Mater.*, 1997, **9**, 3052–3059.